Invited Paper

State-of-the-art Type II Antimonide-based superlattice photodiodes for infrared detection and imaging.

Manijeh Razeghi[a)], Binh-Minh Nguyen, Pierre-Yves Delaunay, Edward Kwei-wei Huang, Siamak Abdollahi Pour, Paritosh Manukar, Simeon Bogdanov.

Center for Quantum Devices, Department of Electrical Engineering and Computer Science, Northwestern University, Evanston, Illinois 60208

Abstract

Type-II InAs/GaSb Superlattice (SL), a system of multi interacting quantum wells was first introduced by Nobel Laureate L. Esaki in the 1970s. Since then, this low dimensional system has drawn a lot of attention for its attractive quantum mechanics properties and its grand potential for the emergence into the application world, especially in infrared detection. In recent years, Type-II InAs/GaSb superlattice photo-detectors have experienced significant improvements in material quality, structural designs and imaging applications which elevated the performances of Type-II InAs/GaSb superlattice photodetectors to a comparable level to the state-of-the-art Mercury Cadmium Telluride. We will present in this talk the current status of the state-of-the-art Type II superlattice photodetectors and focal plane arrays, and the future outlook for this material system.

Keywords: Type II superlattice, InAs/GaSb, M-structure, photodetectors, MWIR, LWIR, VLWIR focal plane arrays.

INTRODUCTION: TYPE II ANTIMONIDE BASED SUPERLATTICES

The Type II InAs/GaSb superlattice was first investigated by Sakaki and Esaki in the 1970s[1] and proposed for infrared detection applications by Smilth and Mailhiot in late 1980s[2]. The superlattice system consists of the material in the 6.1A family (InAs/GaSb/AlSb) which are closely lattice matched to each other and have a type II mis-alligned band offsets between InAs and GaSb. The conduction band level of InAs is lower than the valance band of GaSb, creating a spatial separation of electrons and holes in InAs/GaSb heterostructure and allowing an effective bandgap varying from 0V to 0.5V in InAs/GaSb superlattices (Figure 1a &b). Recently, AlSb, the third member of the 6.1A family was incorporated into the conventional InAs/GaSb superlattice to a new superlattice design called M-structure superlattice (Figure 1c)[3]. The AlSb layer is inserted in the middle of the GaSb layer, creating potential barriers for both electrons and holes. This potential barrier has been shown to signfificantly enhance the carrier effective mass and provide a more flexible control of the conduction and valence band edges[4-6].

[a)] Email: razeghi@eecs.northwestern.edu

Nanophotonics and Macrophotonics for Space Environments III, edited by Edward W. Taylor, David A. Cardimona,
Proc. of SPIE Vol. 7467, 74670T · © 2009 SPIE · CCC code: 0277-786X/09/$18 · doi: 10.1117/12.828421

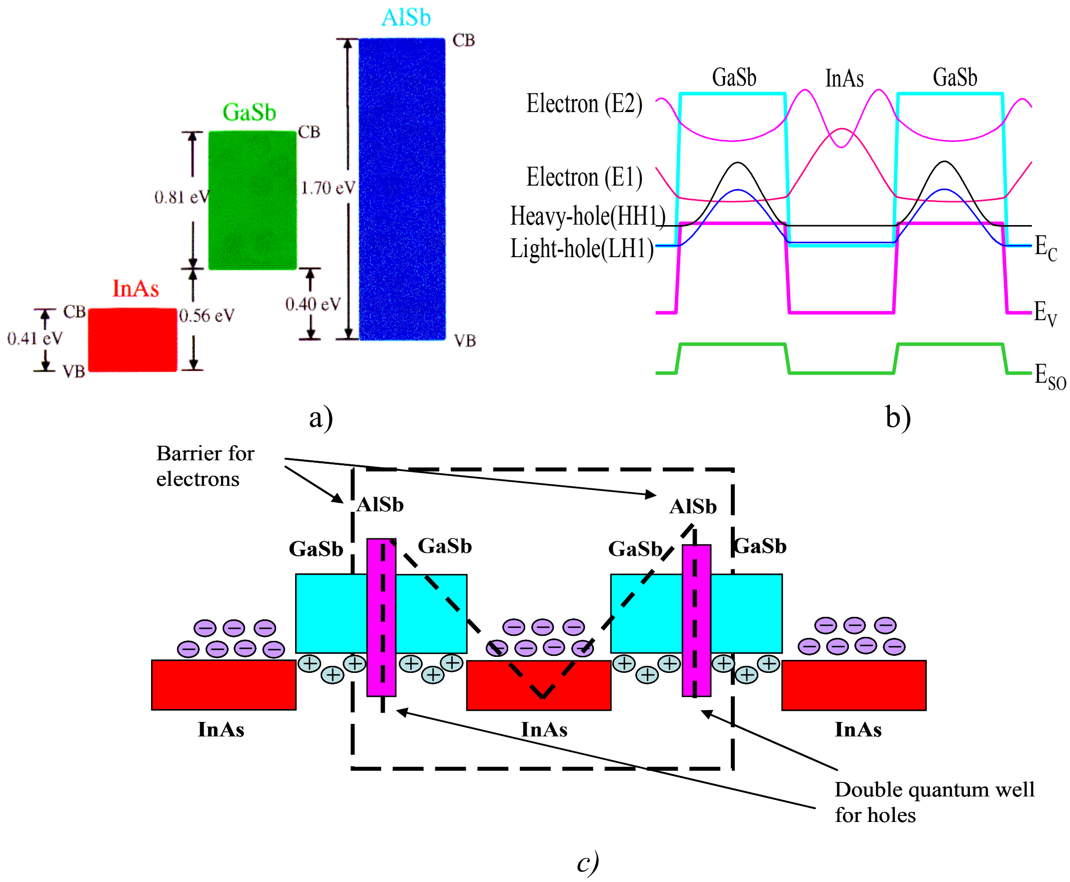

Figure 1 *(a) Band alignment of three constituents of the Type II GEM: InAs, GaSb and AlSb. b) Wave functions of electrons and holes in the InAs/GaSb GEM which enables a flexible control of energy gap, c) A novel GEM material, called M-structure, with large effective mass and flexible tunability of band edge energies thanks to the presence of AlSb layer in the superlattice.*

Compared with the state-of-the-art Mecury Cadmium Telluride technology for infrared detection, Type II superlattice, especially M-structure superlattice benefits from a larger effective mass and the flexibility of controlling the energy gap by atomically engineering the superlattice interfaces and layer thicknesses. Using the same techniques, the Auger recombination rate can be significantly reduced[7]. Despite the potential benefits, Type II superlattice did not really enter the field of infrared detection until the realization of high-quality growth using the state-of-the-art technique of molecular-beam epitaxy (MBE) in the late 1990s. Rapid developments of material quality during the last decade have demonstrated other practical advantages of this material system: covalent-bond stable material, high purity, low defect density, excellent uniformity and high reproducibility. Different photodetector architectures have been utilized to profit from the unique advantages of Type II superlattice, leading to the demonstration of high quality focal plane arrays with comparable performance to the state-of-the-art Mercury Cadmium Telluride technology.

The Center for Quantum Devices is one of the world pioneers in the field of Type II superlattice photon detectors. We were the first to demonstrate the concept of focal plane arrays based Type II superlattices at various infrared wavelengths and still hold the records for highest imaging quality. In this paper, we will discuss the current status of the state-of-the-art Type II superlattice photodetectors and focal plane arrays, and the future outlook for this material system.

MID-INFRARED PHOTO-DETECTORS AND FOCAL PLANE ARRAYS

The main challenges for MWIR detection is the selection of superlattice design. The relatively large energy gap (~200-250meV) requires the superlattice to have thin InAs layer in order to push up the conduction band of the superlattice with respect to the conduction band of the InAs well. In InAs/GaSb superlattices, the InAs layer is -0.6% lattice mismatch to the GaSb substrate and its stress is normally compensated by two InSb interfaces that are +7.6% lattice mismatched to GaSb. But for the MWIR design, the very thin layer of InAs is not enough to cancel the excessive compressive strain from the interfaces, which makes the superlattice highly stressed. This large lattice mismatch will prevent the growth of high quality material, especially if thick structures are required. To solve the problem, a new interface engineering method was invented. By using a small proportion of Gallium in the InSb interfaces, the average lattice constant of the interfaces is reduced, bringing the average lattice constant of superlattice closer to that of the GaSb substrate. The compressive strain of the structure will be completely suppressed, allowing for higher material quality. A clear advantage of using $Ga_xIn_{1-x}Sb$ type interfaces is that it is highly controllable and highly repeatable because of the non-volatility of the Ga and In species on the sample surface at a growth temperature close to 400 °C. The calculation of mixed interface superlattices is performed in the Empirical Tight Binding frame work[8], with variation of the Gallium molar fraction x_1 and x_2 at the two $Ga_xIn_{1-x}Sb$ interfaces. As an example for superlattice consisting of $[(InAs)_7\text{-}Ga_{x1}In_{1-x1}Sb\text{-}(GaSb)_{11}\text{-}Ga_{x2}In_{1-x2}Sb]_N$, **Figure 2**a shows the calculated map of cutoff wavelength in the full range for x_1 and x_2 (from 0 to 1). The cutoff wavelength can range from 3.68 μm to 4.20 μm, which corresponds to an energy variation of ~40 meV. The calculated map of mismatch (absolute values) is shown in **Figure 2**b. It is clear that there exists a zero mismatch composition line. With almost zero lattice mismatch, superlattice of very high crystalline quality can be grown with significant thickness in the microns range.

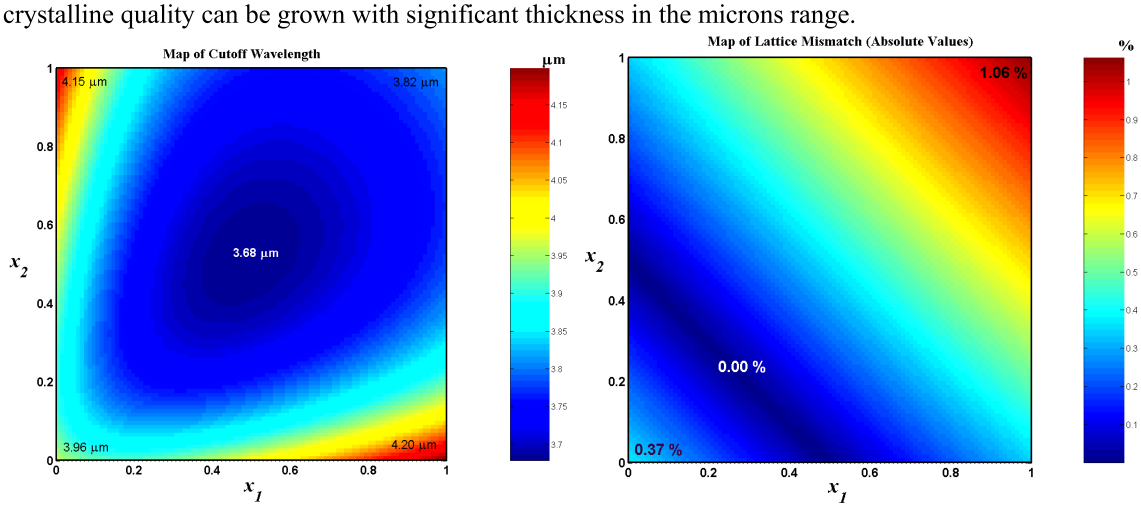

Figure 2- (a) The calculated map of cutoff wavelength for superlattice of $[(InAs)_7\text{-}Ga_{x1}In_{1-x1}Sb\text{-}(GaSb)_{11}\text{-}Ga_{x2}In_{1-x2}Sb]_N$. The cutoff wavelength varies between 3.68-4.20 μm, corresponding to an energy difference of ~40 meV. (b)The calculated map of the absolute values for the lattice mismatch in between the superlattice of $[(InAs)_7\text{-}Ga_{x1}In_{1-x1}Sb\text{-}(GaSb)_{11}\text{-}Ga_{x2}In_{1-x2}Sb]_N$ and the GaSb (001) substrate. Within a narrow stripe like region, zero lattice mismatch can be obtained.

Optimal superlattice design was grown using an Intevac Modular Gen II molecular beam epitaxy system equipped with As and Sb valved cracker sources, on *p*-type epi-ready GaSb (001) substrates. Growths were performed mostly on quarter and whole 2" wafers for both large size detectors and focal plane array processing. The lattice mismatch to the GaSb substrate was controlled below 0.1%. The surface morphology of the samples was studied with a Digital Instruments Nanoscope IIIa atomic force microscope (AFM). The root mean square (RMS) roughness for typical superlattice growths has been demonstrated below 1.5 Å over an area of 20 μm×20 μm. Transmission electron microscope (TEM) characterization was performed for some of our samples through collaboration with WPAFB. A typical TEM image of a superlattice sample shown in Figure 3 confirms the expected layer thickness of each individual layer and the interface sharpness.

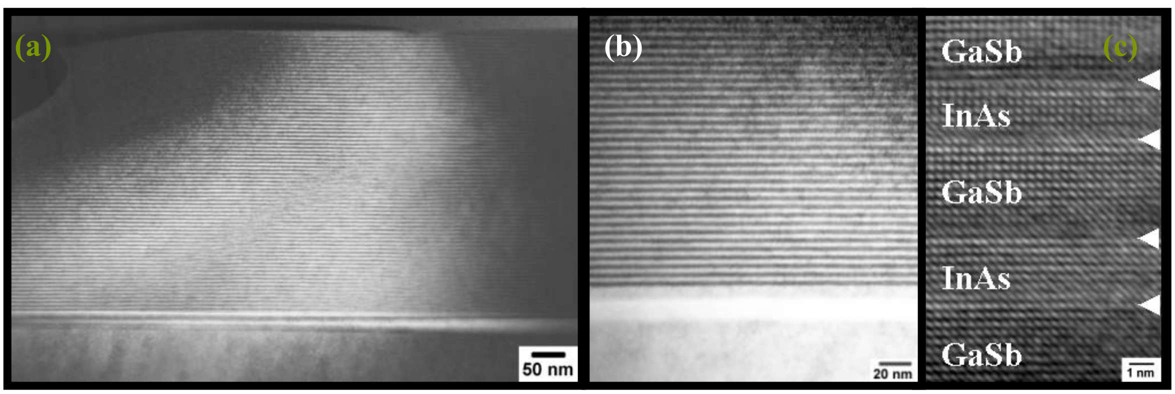

Figure 3- Transmission electron microscope images of a superlattice structure: (a) the entire grown structure (the irregular layer below the superlattice might be due to AlSb oxidation during sample preparation, or due to cleaving); (b) clear uniform atomic layers; (c) close-up view of individual layers and position of interfaces that we received from *WPAFB*.

The typical N-on-P device structure was shown in Figure 4a. The device consists of two 0.5μm thick p and n-contact and an intentionally undoped i-region. The background concentration, measured via Capacitance-Voltage technique[9], could be as low as $5x10^{-14}cm^{-3}$. This low background doping level is a good indication for high material quality, which allows for a long carrier diffusion length and high optical response. Device with 4μm thick i-region exhibits a quantum efficiency in excess of 50% at λ=3.5μm (Figure 4b). Higher quantum efficiency can be obtained by simply growing thicker device as the diffusion length is expected to be much longer than the device's length[10]. However, the low background concentration means higher minority carrier concentration, which leads to a strong diffusion dark current, especially at high temperature.

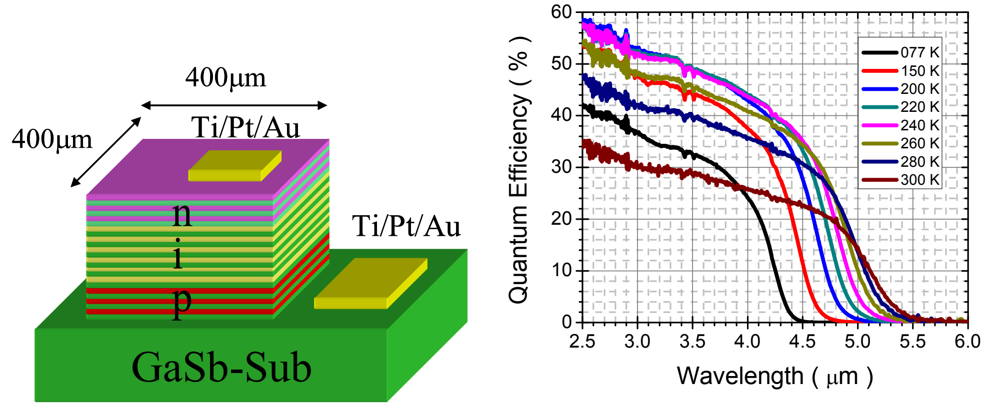

Figure 4- a) Schematic diagram of a Type II superlattice photodiode. B) Quantum efficiency spectrum of a MWIR photodiode at different measured temperatures.

In order to improve the electrical performance of the device, we intentionally p-dope the active region with Beryllium in the InAs layer. Higher doping concentration reduces the minority carrier density, thus lowering the dark current due to the diffusion mechanism. As shown in **Figure 5**a, by doping the active region p-type, the differential resistance of the device could be improved by one order of magnitude.

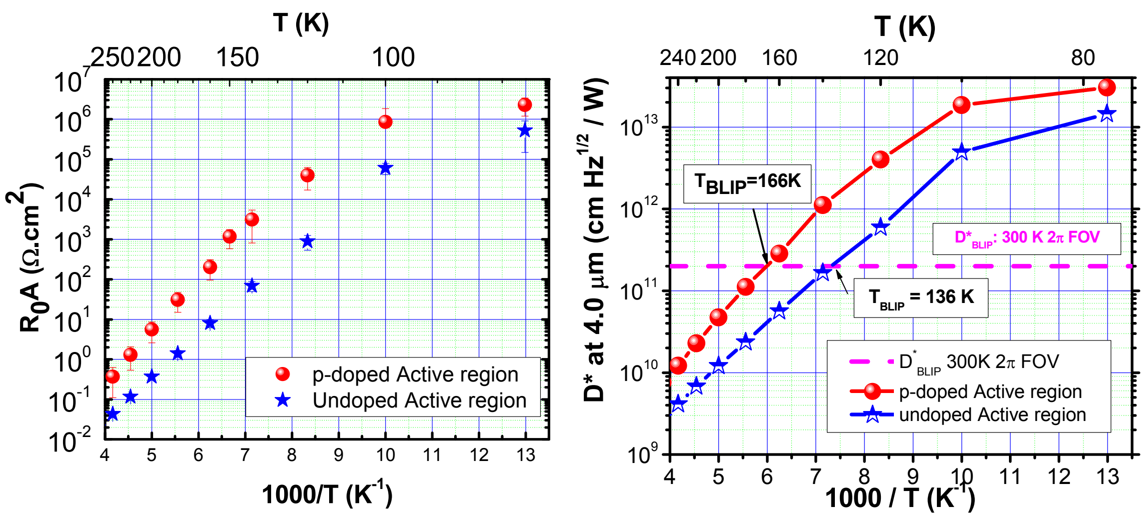

a) **b)**

Figure 5-Comparison of (a)-differential resistance and (b) specific detectivity between intrinsically-undoped devices and intentionally p-doped devices.

The overall performance of the device is shown in **Figure 5**b,. The detectivity of undoped devices attains $1.5\text{x}10^{13}$ cm.Hz$^{1/2}$/W at 77K but decreases rapidly with increased temperature due to the decrease of R_0A and the increase of the dark current. The background limited performance (BLIP) with a 300K-background is achieved at temperature below 136K. By intentionally p-doped the active region, the detectivity at 77K reaches $3\text{x}10^{13}$ cm.Hz$^{1/2}$/W and the BLIP temperature rises to 166K.

Figure 6-Pictures realized with the MWIR FPA at 81K (left) and room temperature (right). The picture on the right is the picture of a soldering iron at 300ºC.

An FPA was processed from this material and hybridized to an Indigo 9705 Read Out Integrated Circuit (ROIC) using indium bumps. The 320x256 array with a 30 µm pitch was tested from 77 to 300K, at a frame rate of 32.64 Hz and an integration time of 22.98 ms. The Noise Equivalent Temperature Difference (NEDT) measured at 81K presented a peak at 10 mK, which is equivalent to the state-of-the-art HgCdTe and QWIP technologies. **Figure 6** shows a representative IR imaging of a MWIR Type II superlattice FPA. The camera is capable to image a human being at up to 150K, and can capture a hot soldering iron at uncooled condition.

LONG WAVELENGTH INFRARED PHOTO-DETECTORS AND FOCAL PLANE ARRAYS

Going toward longer detection wavelength, the energy gap gets smaller and smaller. The material therefore becomes more and more sensitive not only to the bulk properties but also to the surface state of the exposed sidewall. The challenge for LWIR detectors is to decrease the bulk dark current as well as the leakage current at the sidewall of the devices simultaneously.

The superlattice design of 13 ML InAs and 7 ML GaSb with forced InSb interfaces was chosen for a desired cut-off wavelength around 11-12 µm. Typical growth consist of a 0.5 µm thick GaSb p+(p~$10PP^{18\ PP}cmPP^{-3\ PP}$) buffer layer, followed by a 0.5 µm thick pPP^{+PP} (p~$10PP^{18PP}$ $cmPP^{-3PP}$) (Be) superlattice region, a slightly p-doped (p~$10PP^{15\ PP}cmPP^{-3PP}$) superlattice layer, a 0.5 µm thick nPP^{+PP} (n~$10PP^{18\ PP}cmPP^{-3PP}$) (Si) region and finished with a thin InAs nPP^{+PP} (Si) contact. Structural characterization with high resolution X-ray diffraction (HRXRD) exhibited high order diffraction satellites and a lattice mismatch to GaSb substrate of less than 500ppm. Measurement with an atomic force microscope (AFM) showed a morphology with long atomic steps and a root-mean-square (RMS) roughness of under 1.5Å over an area of 20×20 μmPP^{2PP} Using this superlattice structure, we demonstrated that it is possible to increase the quantum efficiency of the devices by growing thicker active regionsTP. Devices with a 6 µm active regions presented a quantum efficiency averaging at 54%[10].

For the optimization of the electrical performance, we have applied the doping method presented in the previous section and have also shown almost one order of magnitude of improvement[11]. However, unlike the case of MWIR, when the doping concentration is too high, LWIR suffers from the tunneling current that was facilitated by the strong built-in electric field and small depletion width. To suppress the tunneling contribution, we have proposed a novel design architecture called p-π-M-n where the M-structure superlattice was inserted in between the standard π and n-regions. This layer has been shown to efficiently reduce the built-in electric field and improve the R_0A by one order of magnitude[4].

As the performance of bulk material and structural design are improved, the surface leakage becomes important and needs to be reduced. An efficient passivation technique needs to be developed in order to transfer the good optical and electrical performances of the devices to smaller detectors. The SiOBB$_{2BB}$ passivation technique used for MWIR detectors has been reported to be inefficient in the LWIR because of the smaller band gap of the superlattice[12]. To solve this issue, a double heterostructure design was proposed with the utilization of two MWIR superlattice contact regions[13]. The higher bandgap of the contacts prevents the charge inversion of carriers at the device sidewall, thus reducing the surface leakage channel. This design has shown the viability of the device with both SiO_2 and polyimide passivation. Electrical testing performed on FPA size devices (25x25 µmPP^{2PP}) showed a complete suppression of the surface leakage. The performances of the small diodes were comparable to the bulk properties of the superlattice.

Recently, the etching techniques to delineate device mesas were intensively studied. It turned out that the damage at the device sidewalls due to plasma dry-etching severely affected the device performance. By developing the etching conditions using the Oxford Plasmalab Inductively Coupled Plasma (ICP) system, we have achieved much smoother sidewall (**Figure 7**c) and better verticality as compared to the conventional dry-etch using Electron Cyclotron Resonance (ECR) (**Figure 7**a) or to a combination of dry-etching and chemical wet-etching(**Figure 7**b).

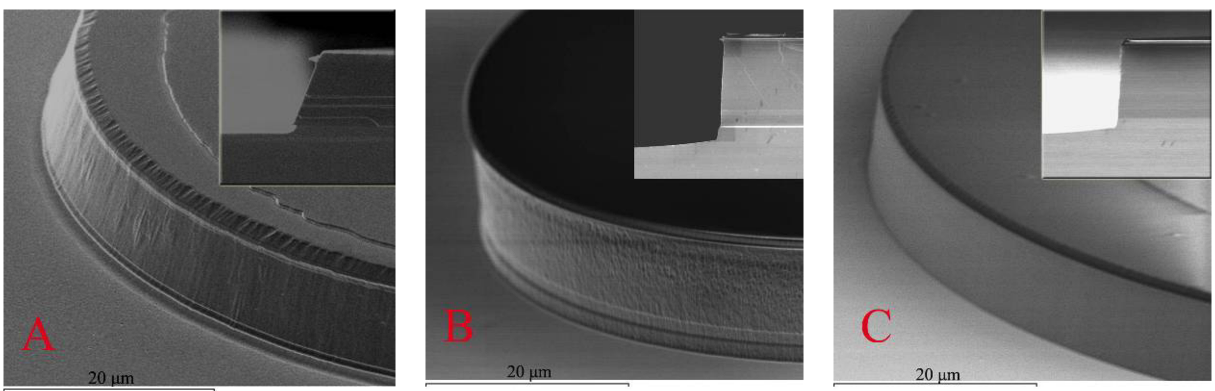

Figure 7- SEM images of 7.7µm deep photodiodes etched by (A) ECR and wet chemical etch, (B) ICP and wet chemical etch and (C) ICP only. The inset of each image shows the resulting sidewall angle to be (A) 70°, (B) 90° and (C) 90°. The samples followed by wet chemical etch show sidewall striations and undercut, whereas (C) is visually smooth.(from REF 14)

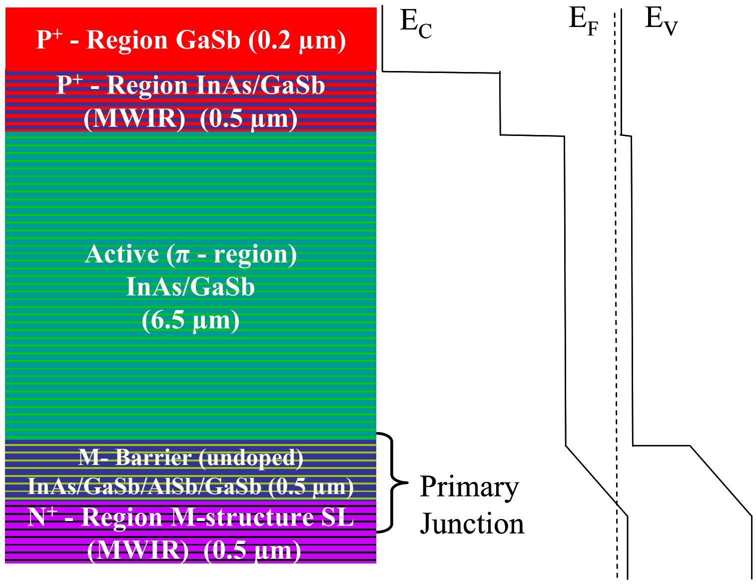

Figure 8-The device structure and band diagram of a $P^+ - \pi - M - N^+$ superlattice photodiode. While the thicker active region increases optical efficiency, the M-barrier and double heterostructure effectively blocks dark current and limits surface leakage.

The schematic diagram of a device design that combines both high optical and high electrical performance is shown in **Figure 8**. A strong optical response and a high quantum efficiency (>50%) were obtained thanks to a long absorption path and high material quality. With help of the M-structure and the double heterostructure design, both bulk dark current and surface leakage current were reduced; at 77K, the device exhibited a dark current level below 5E-5 A/cm^2 at 50mV reverse bias and a surface resistivity ~40kΩ.cm. However, this value is not yet the true performance of the material. Using the ICP etching technique, the same material exhibited almost one order of magnitude decrease of the dark current. **Figure 9** shows the dark current density of the devices processed with ICP, and passivated with different techniques. It appears that the combination of ICP etching and polyimide passivation provide the best electrical performance. However, the discrepancy between different sized diodes indicates that the device performance is still limited by the surface leakage.

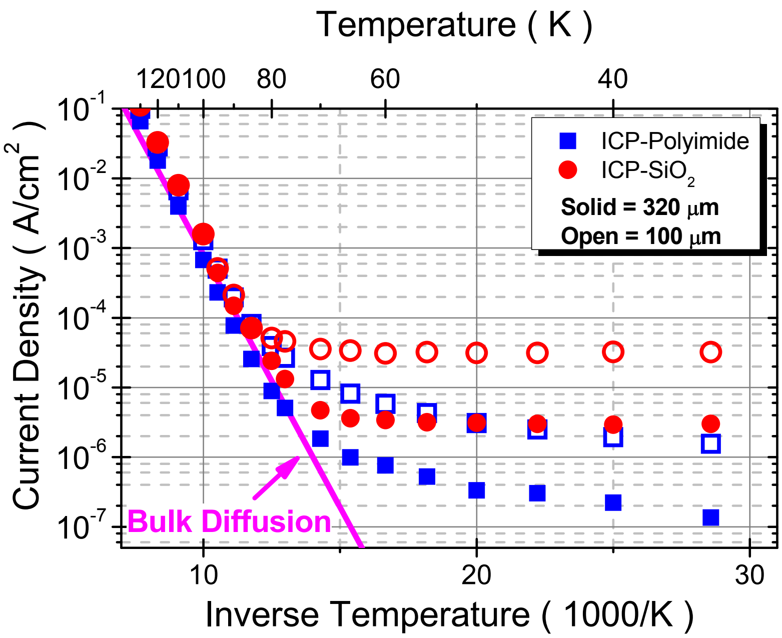

Figure 9-Dark current density temperature dependent measurements of 320µm (solid data point) and 100µm (open data point) diameter diodes for all three samples are shown at 50mV reverse bias. A combination of ICP etching and Polyimide passivation appears to have the best electrical performance. However, the discrepancy between different sized diodes indicates that the device performance is still limited by the surface leakage.

A LWIR FPA was fabricated using the same Indigo ROIC and tested at 81K. The substrate was fully removed in order to enhance the quantum efficiency and the reliability of the array. The deposition of an anti-reflective coating with ion beam deposition increases the quantum efficiency to 89% (**Figure 10**a). The frame rate and the integration time were respectively set at 32.64 Hz and 0.128 ms. The mean NEDT was measured as 23 mK (Figure 10b), corresponding to an operability over 97%. Pictures taken with the 320x256 array at 81K are presented in Figure 11.

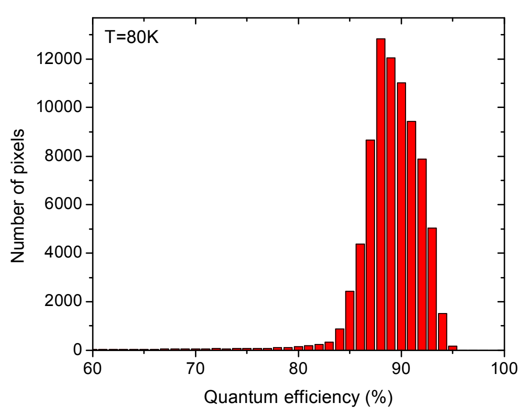

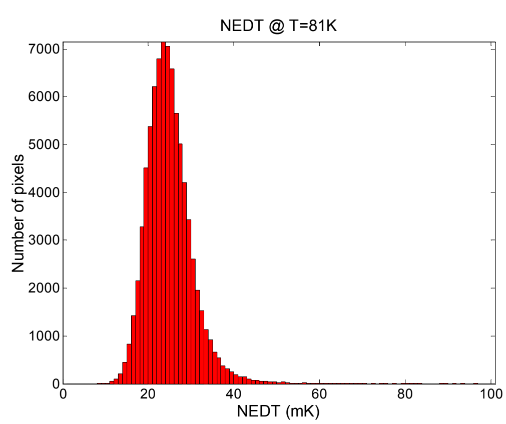

Figure 10-a) Quantum Efficiency and b) NEDT histograms of the LWIR FPA realized at ~80K.

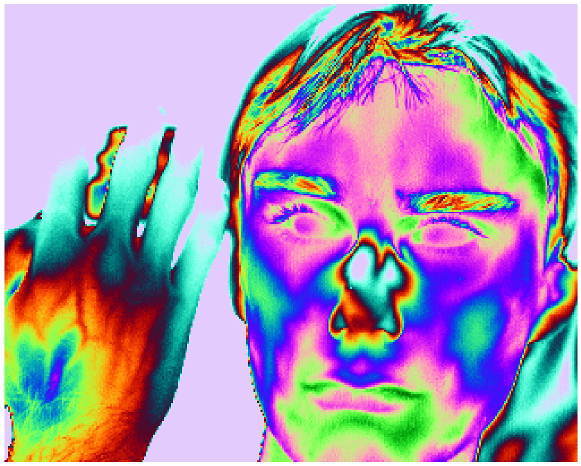

Figure 11- Picture realized with the LWIR FPA at ~80K. The cutoff wavelength of the FPA is 10 µm.

VERY LONG WAVELENGTH INFRARED PHOTODETECTORS

Similar design was applied for VLWIR device with a cut-off wavelength around 14µm. The superlattice is composed of 16MLs InAs and 9 MLs of GaSb, with a nominal bandgap of 80meV. However, the same M-structure used in the LWIR design appears to have a higher conduction band than the VLWIR design. As a consequence, the photo generated electron at the π-region could not get to the n-region to contribute to the photo current, leading to a quantum efficiency as low as 1%.

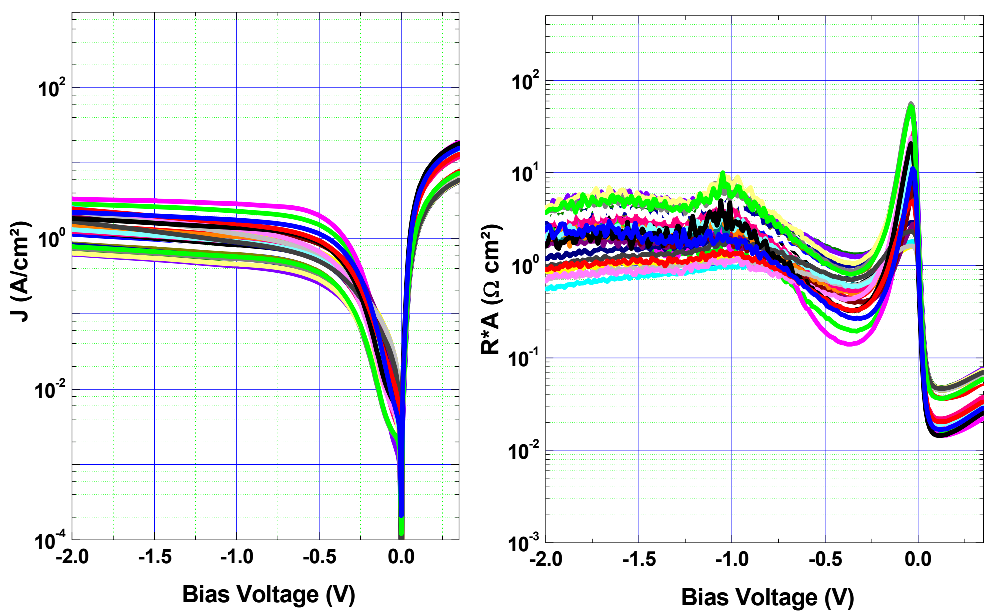

Figure 12- Electrical performance at 77K of a VLWIR device with M-structure barrier.

A similar effect was observed for the diffusion current of electron from the π-side to the n-contact. The barrier in the conduction band has reduced the dark current level more than one order of magnitude, and exhibits an R_0A above 5 Ohm.cm^2 (Figure 12). This design, although has poor optical efficiency, appears to have excellent electrical performance, and might be used in applications that requires high impedance, such as Focal Plane Arrays with commercial ROIC designed for MWIR devices.

In order to improve the quantum efficiency of the device, we have developed many techniques to suppress the effect of the barrier in the conduction band while keeping the same barrier in the valence band. By modifying M-structure design, we can select designs that have absolutely zero band discontinuity between M-structure and the Type II superlattice. Another method is to keep the M-structure design that have the highest effective mass, and adjust the doping level of the barrier such that the barrier width is significantly reduce, allowing for the conduction band tunneling from the p-side to the n-side. As a consequence, a compromise between optical and electrical performance was obtained. In Figure 13, a VLWIR device with a 14.3 μm cut-off exhibited a quantum efficiency of 37% and an R_0A of 2.1 Ohm.cm^2. The specific detectivity attains ~4×10^{10} cm.Hz$^{1/2}$/W at 77K indicating the Background Limited Performance (BLIP) of the device with a 300K background. This performance, without passivation protection and without AR-coating for the enhancement of the optical efficiency, is equivalent to the best reported value for the state-of-the-art HgCdTe at this wavelength.

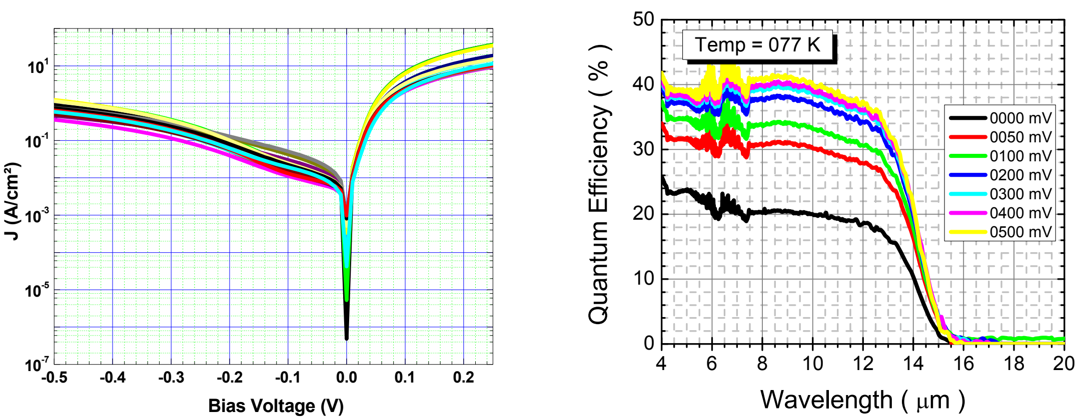

Figure 13- a) Electrical and b) Optical characterization of a VLWIR device optimized for the over all performance.

CONCLUSION

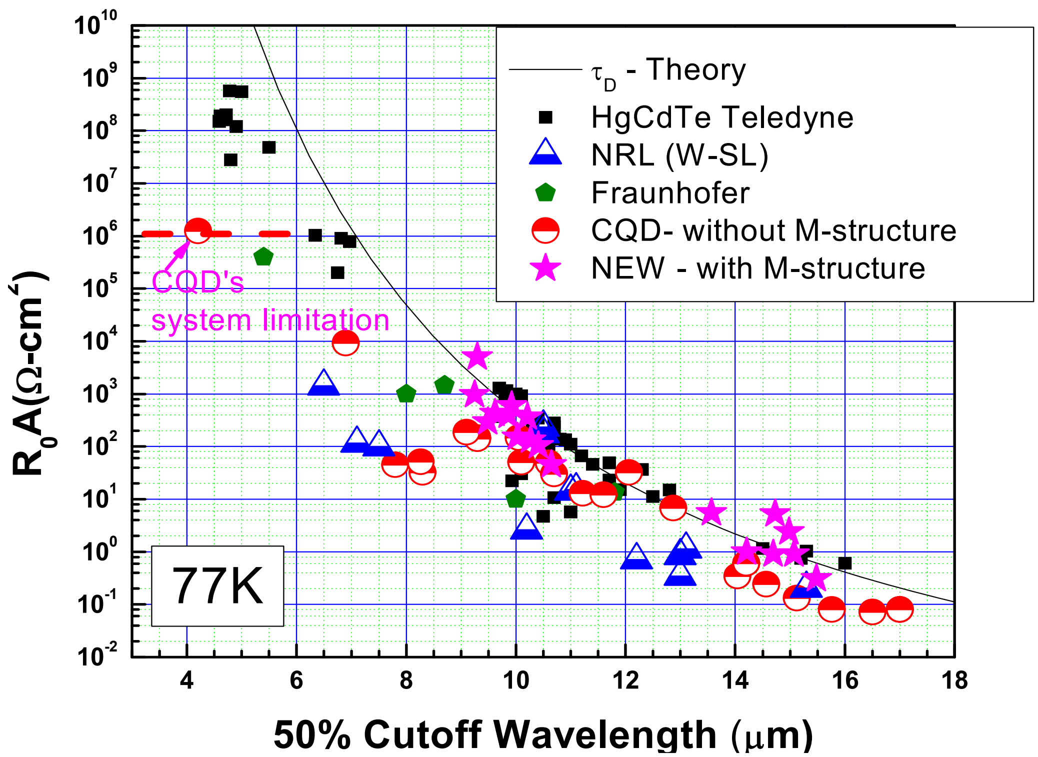

Figure 14- Differential resistance of Type II superlattice photodiodes as a function of cut-off wavelength.

In summary, we have presented the current status of Type-II InAs/GaSb photo-detectors fabricated at the Center for Quantum Devices. Photodiodes with high electrical performances and good optical responsivity have been demonstrated in a wide infrared spectrum, from the MWIR to the VLWIR. High quality Focal Plane Arrays have At the LWIR and VLWIR, Type II superlattices have exhibited comparable and better performance than the state-of-the-art HgCdTe technology (Figure 14). However, Type II superlattice has not yet been seen to reach its theoretical limit. Besides the incremental development of device performance and the extension to longer cut-off wavelength, two main challenges for Type II superlattice to enter the third generation imagers are: (1) the realization of superlattice on large size GaAs or Silicon substrates for cost reduction and mass production and (2) the realization of bi-spectral or multi-spectral focal plane arrays for better dynamic range and better contrast. Initial attempts in the last few years have resulted in promising results, including the demonstration of the first BLIP limited MWIR Type II superlattice photodiode grown on GaAs substrate[15], or the demonstration of MWIR-MWIR two color FPA[16] and the concept of LWIR-LWIR two color detection[17]. If progress could be made at the same rate as recent years, Type II superlattice would definitely outperform the HgCdTe technology and become the material of choice for the third generation of infrared detectors.

REFERENCES

1 G. A. Sai-Halasz, R. Tsu, and L. Esaki, Applied Physics Letters **30** (12), 651 (1977).

2 D. L. Smith and C. Mailhiot, Journal of Applied Physics **62** (6), 2545 (1987).

[3] B. M. Nguyen, M. Razeghi, V. Nathan, and G. J. Brown, *Quantum Sensing and Nanophotonic Devices IV*, (San Jose, CA, USA), 2007,p 64790S

[4] B.-M. Nguyen, D. Hoffman, P.-Y. Delaunay, and M. Razeghi, Applied Physics Letters **91** (16), 163511 (2007).

[5] D. Hoffman, B.-M. Nguyen, E. K.-w. Huang, P.-Y. Delaunay, M. Razeghi, M. Z. Tidrow, and J. Pellegrino, Applied Physics Letters **93** (3), 031107 (2008).

[6] B.-M. Nguyen, D. Hoffman, P.-Y. Delaunay, E. K.-W. Huang, M. Razeghi, and J. Pellegrino, Applied Physics Letters **93** (16), 163502 (2008).

[7] H. Mohseni, V. I. Litvinov, and M. Razeghi, Physical Review B (Condensed Matter and Materials Physics) **58** (23), 15378 (1998).

[8] Y. Wei and M. Razeghi, Physical Review B (Condensed Matter and Materials Physics) **69** (8), 085316 (2004).

[9] A. Hood, D. Hoffman, Y. Wei, F. Fuchs, and M. Razeghi, Applied Physics Letters **88** (5), 052112 (2006).

[10] B.-M. Nguyen, D. Hoffman, Y. Wei, P.-Y. Delaunay, A. Hood, and M. Razeghi, Applied Physics Letters **90** (23), 231108 (2007).

[11] D. Hoffman, B.-M. Nguyen, P.-Y. Delaunay, A. Hood, M. Razeghi, and J. Pellegrino, Applied Physics Letters **91** (14), 143507 (2007).

[12] R. Rehm, M. Walther, F. Fuchs, J. Schmitz, and J. Fleissner, Applied Physics Letters **86** (17), 173501 (2005).

[13] P.-Y. Delaunay, A. Hood, B. M. Nguyen, D. Hoffman, Y. Wei, and M. Razeghi, Applied Physics Letters **91** (9), 091112 (2007).

[14] E. K.-w. Huang, D. Hoffman, B.-M. Nguyen, P.-Y. Delaunay, and M. Razeghi, Applied Physics Letters **94** (5), 053506 (2009).

[15] B.-M. Nguyen, D. Hoffman, E. K. Huang, P.-Y. Delaunay, and M. Razeghi, *Infrared Technology and Applications XXXV*, (Orlando, FL, USA), 2009,p 72981T

[16] R. Rehm, M. Walther, J. Schmitz, F. Rutz, J. Fleissner, R. Scheibner, and J. Ziegler, *Quantum Sensing and Nanophotonic Devices VI*, (San Jose, CA, USA), 2009,p 72220T

[17] P.-Y. Delaunay, B.-M. Nguyen, D. Hoffman, A. Hood, E. K.-W. Huang, M. Razeghi, and M. Z. Tidrow, Applied Physics Letters **92** (11), 111112 (2008).